Linear Size Contraction of Ligand Protected Ag_{29} Clusters by Substituting Ag with Cu

Ananya Baksi,*[,⊥] Erik Karsten Schneider,[⊥] Patrick Weis, Indranath Chakraborty, Olaf Fuhr, Sergei Lebedkin, Wolfgang J. Parak, and Manfred M. Kappes*

ABSTRACT: **There are only a few examples of atomically precise, ligand protected, bimetallic coinage metal clusters in which molecular structure remains essentially unchanged over a wide composition range starting from the corresponding homometallic species. Such model systems are particularly useful to study the dynamics of alloy formation on the nanoscale. Here we demonstrate the unusual reactivity of solvated metalloid superatom $Ag_{29}(BDT)_{12}(PPh_3)_4$ (BDT = 1,3 benzenedithiol) clusters toward semiconducting $Cu_{12}S_6(DPPPT)_4$ (DPPPT = bis (diphenylphosphino)pentane) clusters as an efficient way to exchange multiple copper atoms into the atomically precise silver clusters without changing overall the structure type. Concentration dependent UV−vis absorption and online mass spectrometry shows that 14 Cu atoms can be exchanged into the silver cluster. Beyond the 14 Cu atom exchange, the cluster degrades to smaller thiolates. Information on cluster structures is obtained from high resolution ion mobility mass spectrometry, which shows a linear decrease in collision cross section (CCS) with each Ag/Cu exchanged. Several isomeric structures are calculated by density functional theory (DFT), and their calculated collision cross sections are used to identify the most stable isomers for each Ag/Cu exchange product. Ag/Cu exchange is essentially limited to the cluster surface/shell. The core appears not to be involved.**

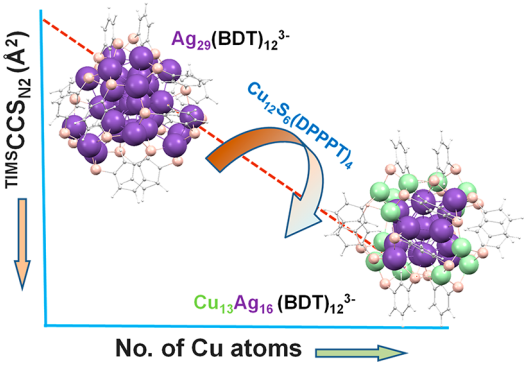

KEYWORDS: *intercluster reaction, Ag−Cu alloy cluster, ion mobility spectrometry, CCS calculation, Ag_{29} cluster, DFT calculation, mass spectrometry*

Atomically precise, bimetallic coinage metal alloy clusters stabilized by thiol ligands are presently being extensively studied due to their tunable structure and properties.[1−4] Among these monolayer protected alloy clusters, the most studied metal combination is Au/Ag as these elements are fully miscible in bulk.[2,5−7] The corresponding alloy clusters often have similar stability compared to the homonuclear parent clusters, but with significantly modified optical and catalytic properties. Although, many stable Au clusters are known and have been well characterized over recent years, stable Ag clusters comprise a rather recent entry to the monolayer protected coinage metal cluster field.[8] At this writing, $Ag_{25}(SR)_{18}$,[9] $Ag_{29}(SR)_{12}$,[10] and $Ag_{44}(SR)_{30}$[11,12] are arguably the extensively studied ones (SR = thiolate).

In contrast to Au/Ag, there are far fewer accounts of Cu containing coinage metal alloy clusters. In the case of $Cu_xAu_{25-x}(SR)_{18}$ (where x = 1−5), Negishi et al. found computationally that Cu atoms occupy the central icosahedron.[13] Recently, Jin et al. have synthesized M_{29}(S Adm)$_{18}(PPh_3)_4$ clusters (M = Ag, Cu, Pd, Pt; S Adm = adamantanethiol) and have shown that a maximum of 16 Cu atoms can be exchanged into the Ag_{29}(S Adm)$_{18}$ cluster and that all Cu atoms occupy positions in the outer shell.[14] There are a few reports of even larger bare Ag−Cu alloy clusters with higher Cu doping such as $Ag_{27}Cu_{13}$ or $Ag_{27}Cu_7$. In all of these cases, Cu atoms appear to occupy positions in the cluster cores.[1]

Intercluster reaction in solution provides an emerging synthetic route to create unusual coinage/transition metal alloy cluster compositions and structures while retaining the overall nuclearity of one (or often even both) of the involved clusters.[15−17] $(AuAg)_{25}(SR)_{18}$, $Au_{12}Ag_{32}(SR)_{30}$,[18] $Ir_3Au_{22}(SR)_{18}$,[19] $(AuAg)_{38}(SR)_{24}$[20,21] are examples of reaction products which have been accessed in this way. From the start,

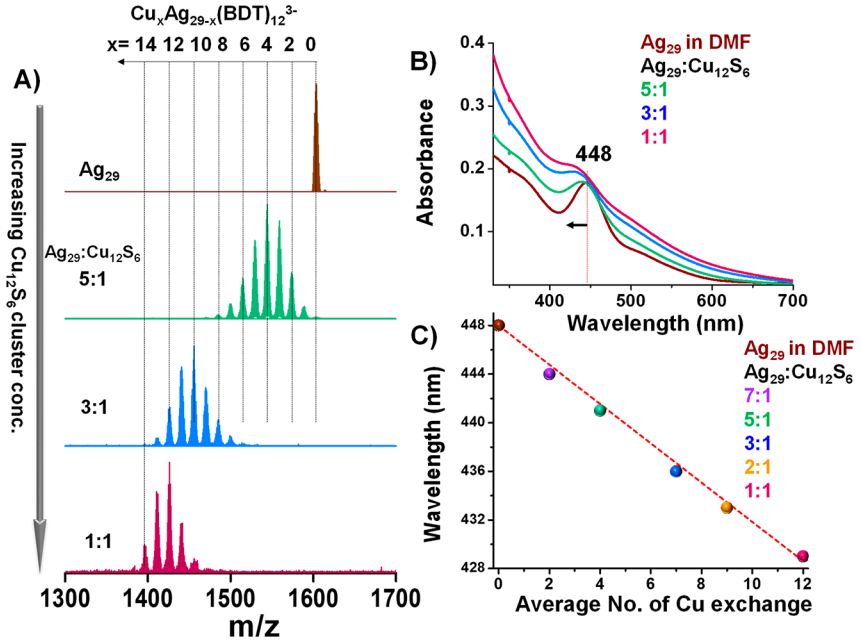

Figure 1. (A) Concentration dependent ESI MS showing an increasing number of Ag/Cu exchanges with increasing relative $Cu_{12}S_6$ cluster concentration. (B) Corresponding UV−vis absorption spectra of the mixture with varying $Ag_{29}/Cu_{12}S_6$ concentration ratios acquired after 10 min of reaction. (C) Position of local near UV absorption maxima versus average number of Ag/Cu exchanges for various concentration ratios as indicated (see text).

mass spectrometry has been an indispensable tool in identifying reaction products formed during intercluster reactions. Coupled with this, ion mobility spectrometry (IMS) has provided structural information on species present in the reaction mixtures, for example, by analyzing isomer mixtures and by identifying cluster dimers.[22,23]

Here we have used higher resolution trapped ion mobility spectrometry (TIMS) to probe the reaction of $Cu_{12}S_6(DPPPT)_4$ clusters[24] in dichloromethane with $Ag_{29}(BDT)_{12}$ (DPPPT = bis(diphenylphosphino)pentane and BDT = 1,3 benzenedithiol) in dimethylformamide solution at room temperature. Upon probing the composition of the 29 atom cluster after solution mixing, we observe exchange of up to 14 Ag atoms by Cu. For each additional exchange of a silver atom by copper, the overall size of the resulting $Ag_{29-x}Cu_x(BDT)_{12}$ cluster as reflected by its gas phase collision cross section (measured by TIMS), decreases roughly linearly with x. Extensive density functional theory (DFT) calculations were carried out to model the corresponding structures. In particular, multiple isomeric forms for a given x were geometry optimized to provide structural models. Trajectory method calculations were then used to predict collision cross sections which in turn allowed rational identification of the isomeric structures occurring by comparison of structural models to TIMS measurements.

RESULTS AND DISCUSSION

Time and Concentration Dependence. $Ag_{29}(BDT)_{12}(PPh_3)_4$[10] and $Cu_{12}S_6(DPPPT)_4$[24] clusters were synthesized following reported methods (see SI for details). For simplicity, we refer to these clusters as Ag_{29} and $Cu_{12}S_6$, respectively, in the following text. The previously determined crystal structure of the $Cu_{12}S_6$ cluster is shown in the Supporting Information (Figure S1). Different concentrations of $Cu_{12}S_6$ clusters (in dichloromethane (DCM)) were added to solutions of 10 μM Ag_{29} cluster (in *N*,*N* dimethylformamide (DMF) to achieve final concentration ratios of 5:1, 3:1, and 1:1, respectively ($Ag_{29}/Cu_{12}S_6$). For each concentration ratio, we recorded UV−vis absorption spectra (Figure S2) and cluster compositions as determined by electrospray ionization mass spectrometry (ESI MS) (Figure S3) in the trianion channel at various times after mixing. Typical ESI MS data acquired after 10 min of reaction are shown in Figure 1A for various concentration ratios.

Even for the lowest relative amount of $Cu_{12}S_6$ up to 9 Cu exchanges were seen. Compared to our recent study of intercluster reaction of $Au_{25}(SR)_{18}$ and $Ag_{44}(SR)_{30}$ cluster species,[25] the reaction was faster and equilibrium was reached more quickly (within 10−15 min). Nevertheless, all reactions were followed for up to 30 min to ensure that no long term changes occurred, for example, due to secondary reactions among the products (Figure S3). At the concentration ratio of 3:1, up to 12 Ag atoms of the 29 atom cluster were exchanged with Cu atoms. This number increased to 14 Ag/Cu exchanges at a 1:1 ratio. Beyond this, the 29 atom cluster started degrading as indicated by the formation of smaller thiolates. Representative concentration dependent UV−vis absorption spectra after 10 min of reaction are shown in Figure 1B. The parent Ag_{29} cluster has a characteristic absorption peak at around 448 nm with a shoulder at 510 nm. The relative intensity of this shoulder decreases with increasing relative $Cu_{12}S_6$ cluster concentration, while at the same time the main 448 nm peak shifts to the blue. This peak position is compared with the average number of Cu exchanges in Figure 1C, indicating a linear decrease (adjusted $R^2 = 0.996$) of about 1.6 nm for each Cu/Ag (exact position was determined by subtracting the baseline). The average numbers are found from the respective mass spectra by fitting a Gaussian intensity distribution to the mixed species and taking its center. In each case, the actual number of Cu exchanged is equivalent to this average number ±3.

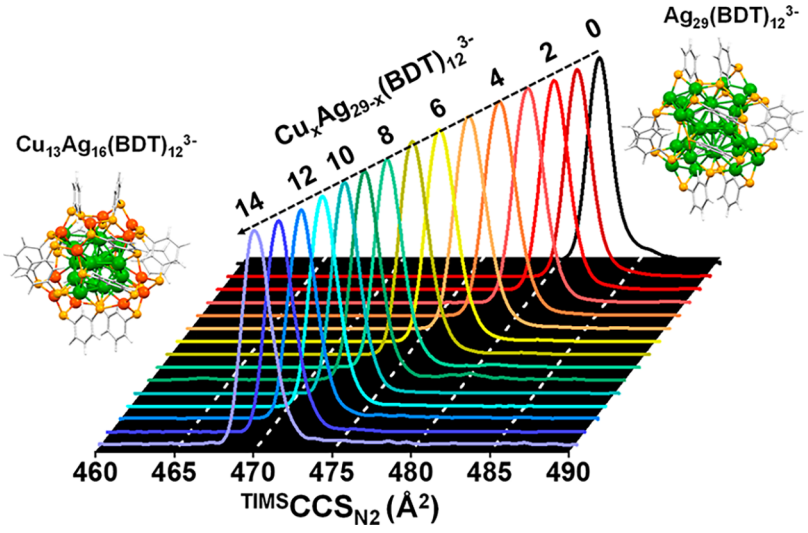

Figure 2. Extracted ion mobilograms, that is, ion intensity versus CCS, determined for $Cu_xAg_{29-x}(BDT)_{12}^{3-}$ (x = 0−14) by tims TOFMS. Note that the size of the cluster decreases linearly with each Ag/Cu exchange by 0.9 Å^2. Shown alongside the measurements are DFT optimized structures of $Ag_{29}(BDT)_{12}^{3-}$ and $Cu_{13}Ag_{16}(BDT)_{12}^{3-}$. Color code: Ag, green; S, orange; Cu, red; C, gray; H, light gray.

Structural Changes. To explore structural changes associated with Ag/Cu exchange in the 29 atom clusters, high resolution TIMS was conducted using a Bruker tims TOF (time of flight) instrument with a mobility resolution in the range of 200−250 and an accuracy of 0.2%.[26,27] As all 0−14 Ag/Cu exchange products could not be accessed at a single concentration, three different concentration ratios (5:1, 3:1, and 1:1) were used to cover the full range of exchange products. Each measurement was repeated to confirm the reproducibility of the measured ion mobility and thus of the collision cross section (CCS) which can be determined from it. The mobilograms observed during these concentration ratio dependent measurements are shown in Figures 2 and S4. Interestingly, we resolve a systematic change in CCS (as measured 10 min after mixing of reagent solutions) with the number of Ag/Cu exchanged. The corresponding experimental CCS values for 0−14 Cu exchanges, that is, for $Cu_xAg_{29-x}(BDT)_{12}^{3-}$ (x = 0−14), are shown in Table 1. Whereas the CCS value of the parent $Ag_{29}(BDT)_{12}^{3-}$ is found to be 482.6 Å^2 (see SI for details), the collision cross section is found to decrease linearly (Figure S5) with each Ag/Cu exchange by about 0.9 Å^2 and reaches a value of 469.9 Å^2 at $Cu_{14}Ag_{15}(BDT)_{12}^{3-}$. Although a linear decrease would seem to be intuitive at first glance considering that the van der Waals radius of a Cu atom is about 12% smaller than Ag, this is less obvious when considering that metal−metal and metal−sulfur bond lengths in coinage metal clusters are quite sensitive to the bonding situation and overall electronic structure.

Nevertheless, the linear decrease points toward exchange of all Ag atoms in chemically similar environments without substantially affecting the overall geometry of the system. Considering the crystal structure of the Ag_{29} cluster, there are four distinguishable positions which Ag atoms can occupy. These are (cf. Figure 3) the central atom in the filled icosahedron core, the other 12 atoms of the icosahedron, another 12 atoms on the cluster shell directly bonded to the S atoms of the ligands, and 4 undercoordinated Ag atoms (to each of which a PPh_3 ligand is bound in the solid, which is lost in solution/gas phase). Assuming a similar core−shell type structure for the nanoalloy clusters considered here, the stability increase driving the exchange reaction could originate from relief of strain *via* variation of atomic size and bond length. Note that the Ag—Ag bond length in Ag_{29} is larger on the shell surface (2.92 Å) than in the icosahedron core (2.77 Å), that is, the core is more compact. To keep the structure intact, that is, core bonds shorter than surface bonds, the smaller Cu atoms might then be expected to be preferentially exchanged into the core. Analogous exchange has previously been inferred to reduce strain in bare Cu and Ni doped Ag clusters.[1] However, this analogy can only justify 13 Cu exchanges, not 14 as observed here. Furthermore, for thiol protected coinage metal clusters, Ag—S versus Cu—S bond lengths and bond strengths also need to be taken into account

Table 1. Experimental CCS Values for $Cu_xAg_{29-x}(BDT)_{12}^{3-}$ (x = 0−14)[a]

no. of Cu exchange	experimental CCS (Å^2)	CCS % w.r.t. Ag_{29}	CCS/ΔCCS
0	482.6	100.00	283
1	481.9	99.85	267
2	481.1	99.69	269
3	480.1	99.48	219
4	478.9	99.23	210
5	477.8	99.01	208
6	476.8	98.80	217
7	476.2	98.67	231
8	474.9	98.40	231
9	474.0	98.22	237
10	473.3	98.07	236
11	472.3	97.88	235
12	471.5	97.70	229
13	470.6	97.51	221
14	469.9	97.37	223

[a](i) Absolute numbers in Å^2 as measured by tims TOFMS in N_2 and (ii) relative numbers in % normalized to the CCS of the parent cluster. CCS/ΔCCS is shown alongside as an indication of effective resolution achieved for each measurement (with ΔCCS taken as the fwhm of the corresponding mobilogram peak). The numbers are in the range of the instrumental resolution indicating very narrow isomer distributions.

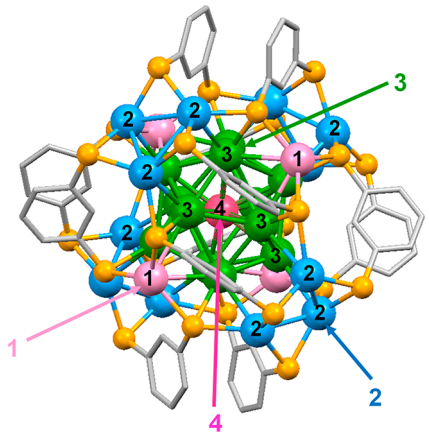

Figure 3. DFT optimized structure of $Ag_{29}(BDT)_{12}^{3-}$ showing four different types of Ag atoms in the cluster for possible Cu exchange locations. The four different types of Ag atoms are labeled with different colors; 4 under coordinated Ag atoms on the surface in light pink, 12 surface Ag atoms directly bonded to the dithiol ligands in blue, 12 Ag atoms of the icosahedron in green, and the center of the icosahedron in dark pink. C and S are shown in gray and orange, respectively. H atoms are removed for clarity.

when considering possible exchange products. Cu—S is the stronger and shorter bond, and on this basis one would therefore expect surface exchange of protected silver clusters to be favorable. Jin and group recently reported up to 16 Cu exchange in the $Ag_{29}(SR)_{18}^{3+}$ system where no Cu was found in the core.[14] The preferential surface position of the 12 Cu atoms was also observed in an X ray crystal structure determination of $Ag_{28}Cu_{12}(SR)_{24}^{4-}$ by Zheng et al.[28] Even in a Cu rich $[Au_{12}Cu_{32}(SPhCF_3)_{30}]^{4-}$ cluster, all 12 Au atoms occupied core positions leaving the Cu atoms outside bonded to the thiolated ligands.[29] In another recent report, Jin and group showed that 70 Cu atoms are preferentially bonded to 55 thiolate ligands on the surface in a $[Au_{52}Cu_{72}(p\text{ MBT})_{55}]^{+}$ (p MBT = SPh p CH_3) cluster.[30] All of these studies point toward the exchange of Cu atoms on the cluster surface rather than in the core. To support such an effect experimentally, we conducted collision induced dissociation (CID) of each of the product trianions by impacting them with N_2 collision gas at a fixed collision energy (laboratory CE = 96 eV). This specific laboratory collision energy was chosen for the parent Ag_{29} cluster to ensure that both the parent ion and the fragments were observed with reasonable intensity. The reported primary anionic fragments of parent $Ag_{29}(BDT)_{12}^{3-}$ clusters are $Ag_5(BDT)_3^{-}$ and $Ag_{24}(BDT)_9^{2-}$ as also shown in Figure S6.[31] With an increasing number of Cu exchanges in the parent ion, more Cu containing fragments are observed. Interestingly, the pure $Ag_5(BDT)_3^{-}$ fragment disappears starting at about $Ag_{21}Cu_8(BDT)_{12}^{3-}$. Furthermore, $Cu_5(BDT)_3^{-}$ fragments can be seen for $Ag_{16-20}Cu_{9-13}(BDT)_{12}^{3-}$ arguing for Cu enrichment of the surface positions of the impacting clusters. The results are summarized in Figure S6.

DFT and CCS Calculations. To rationally correlate the experimentally observed CCS and the corresponding probable Cu exchange positions in the Ag_{29} system, extensive density functional theory (DFT) calculations were carried out. Initially, the structure of $Ag_{29}(BDT)_{12}^{3-}$ was optimized using

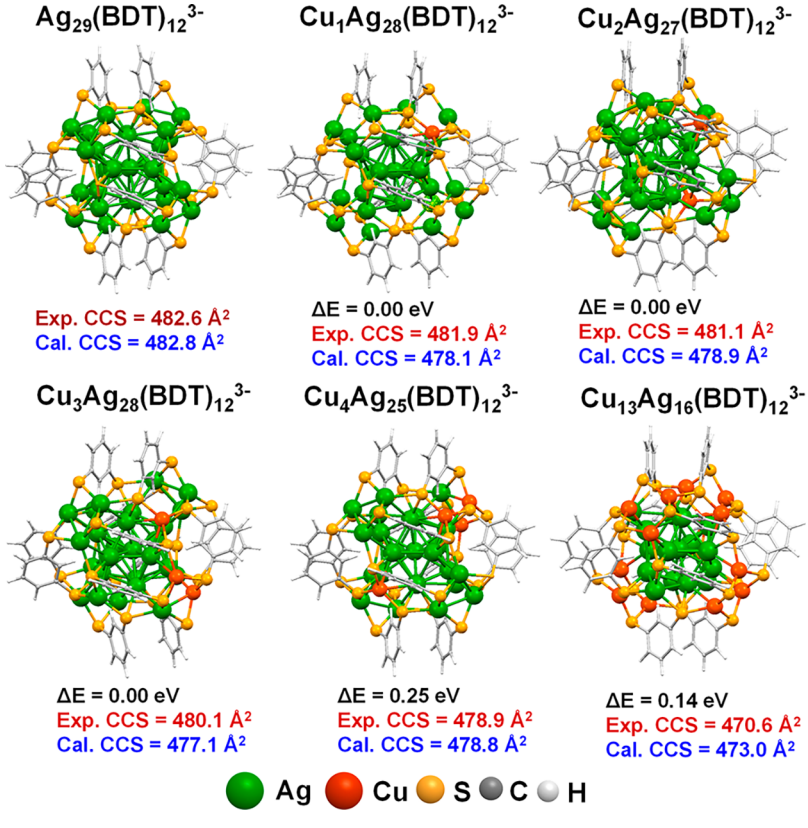

Figure 4. DFT optimized structure of the most probable isomer (lowest energy and/or best fitting scaled cross section among those considered) for various Cu exchanged products as indicated. All other isomers considered at the DFT level for each Cu exchange product are shown in Supporting Information. Coordinates of the optimized structures are given in Supporting Information Tables S3−S9.

the BP 86[32] functional and def2 SVP[33] basis set as implemented in the recent version of Turbomole[34] with a starting structure based on Bakr et al.[10] After removal of the phosphines and energy minimization under constrained symmetry,[35] a CCS value was calculated using the trajectory method as implemented in the IMoS software (details in the Experimental Section in the Supporting Information).[36,37] In the case of N_2 as a drift gas, the charge distribution needs to be considered,[38] therefore a natural population analysis (NPA)[39] analysis was run after the structures had converged. The calculated CCS without scaling was 484.8 Å^2, which compares with an experimentally determined $^{TIMS}CCS_{N2}$ value of 482.6 Å^2. The difference can be rationalized by Ag not being properly parametrized in the standard parameters of IMoS. Hence, we used the known structure of Ag_{29} as a calibrant and scaled all subsequent CCS calculations with a factor of 482.6/484.8 = 0.995 (for all $Cu_xAg_{29-x}(BDT)_{12}^{3-}$ treated). Details regarding the structure optimization, the CCS calculation, and the scaling can be found in the SI. The optimized $Ag_{29}(BDT)_{12}^{3-}$ DFT structure was used as a starting point for the structure calculation of the (Ag/Cu) alloy clusters, where first one Ag atom was replaced by Cu resulting in four different isomers (corresponding to the four different Ag positions as discussed above) and the geometry optimization was performed without symmetry restrictions.

The four resulting $CuAg_{28}(BDT)_{12}^{3-}$ isomers are shown in Figure S7. The most stable isomer corresponds to isomer 1 (also shown in Figure 4) in which Cu is exchanged with one of the four undercoordinated Ag atoms (position 1 in Figure 3). Its calculated scaled CCS is also close to the observed one. A similar (but now combinatorial) treatment for two Cu exchanges resulted in 19 possible isomers each of which was calculated at the DFT level along with their scaled CCS values (Figure S8). The calculated scaled CCS of the lowest energy isomer (Isomer 3 in Figure S8) was found to be close to the experimentally observed one. Similarly, six of the possible isomers were calculated for $Cu_3Ag_{26}(BDT)_{12}^{3-}$ and $Cu_4Ag_{25}(BDT)_{12}^{3-}$. They are shown in Figures S9 and S10, respectfully. Typically, the best CCS fit was found when most of the Cu atoms occupied surface positions. It should be noted that, in all cases, the total energy difference among the isomers considered for a given number of exchanged coppers was always less than 2 eV which is small considering the comparatively large size of the cluster. Hence, it would be difficult to predict a possible Cu exchange position solely based on DFT without the CCS data. The most probable isomers of various different Cu exchange products (x = 1, 2, 3, 4, and 13) are shown in Figure 4. All isomers considered for the individual products are shown in Figures S7–S13. We infer from the structure CCS correlation of the first four Cu exchanged products that Cu exchange occurs on the surface. To reduce the computation cost, the structures of all intermediate Cu exchange products $Cu_xAg_{29-x}(BDT)_{12}^{3-}$ (x = 5–11) were not calculated. The energy change due to each Cu exchange and various isomers are listed in Table S1.

In the case of $Cu_{12}Ag_{17}(BDT)_{12}^{3-}$, the most stable isomer of those considered was found to be the one where all 12 surface Ag atoms (except the undercoordinated ones, position 2 as shown in Figure 3) are exchanged with Cu (Figure S11). The scaled CCS calculated for this isomer also matched the experimental value quite well. For $Cu_{13}Ag_{16}(BDT)_{12}^{3-}$, 11 possible isomers (Figure S12 and associated Table S2) were considered: Surface 1–6, no Cu atoms in the icosahedron core (ΔE = 0.00–0.14 eV); Arbitrary 1–4, arbitrary distribution of the Cu atoms in all possible positions (ΔE = 0.43–0.76 eV); and Icosahedron core, all 13 Cu atoms in the icosahedron core (ΔE = 2.11 eV). The calculated scaled CCS values of these isomers were found to be in the range of 473.0–481.8 Å^2 while the experimentally observed CCS was 470.6 Å^2. A plot of calculated scaled CCS against ΔE is shown in Figure S13. Surface 1, which is slightly higher in energy compared to the most stable isomer, is the best fitting structure for $Cu_{13}Ag_{16}(BDT)_{12}^{3-}$, in agreement with the surface exchange trend of individual Cu exchange products as discussed above.

CONCLUSION

In summary, we show an approach to exchange about 50% of the Ag atoms in highly stable, ligand protected Ag_{29} clusters following intercluster reaction with another highly stable $Cu_{12}S_6$ cluster in solution. This is an example of an intercluster reaction involving species with significantly disparate nominal oxidation states (Ag atoms in Ag_{29} are either in Ag(0) or Ag(I); all Cu atoms in $Cu_{12}S_6$ are Cu(I)). Up to 14 Cu exchanges were observed for a 1:1 concentration ratio of the two reacting clusters which were monitored in parallel by UV–vis absorption spectroscopy and negative ion mobility mass spectrometry. Detailed tims TOF measurements revealed a linear size contraction as increasing numbers of Ag atoms were exchanged with Cu. Extensive density functional theory (DFT) calculations followed by trajectory method CCS simulations rationally identify the most probable species among several possible isomers for a given number of Cu exchanges. We conclude that DFT alone cannot confirm the exact Cu exchange position, as in all cases considered the energy difference between plausible $Cu_xAg_{29-x}(BDT)_{12}^{3-}$ isomers was less than 2 eV. Considering the size of the ligand protected cluster molecules this is likely approaching the error of the calculation. However, DFT coupled with high resolution ion mobility spectrometry can distinguish such species rationally and allows us to conclude that in this intercluster reaction system over the composition range probed the overall structure of the 29 atom cluster does not significantly change, whereas Ag/Cu exchange is essentially limited to its surface/shell. The core appears not to be involved.

EXPERIMENTAL SECTION

Synthesis of Ag_{29} and $Cu_{12}S_6$ Clusters. $Ag_{29}(BDT)_{12}(TPP)_4$ clusters were synthesized following a reported method by Bakr et al.[10] $Cu_{12}S_6(DPPPT)_4$ clusters were synthesized following the method reported by Yang et al.[24] Synthesis of these clusters is detailed in the Supporting Information.

Mass Spectrometry. All of the IMS measurements were performed using a commercially available Bruker timsTOF. TIMS is an IMS variant which determines ion mobilities with particularly high resolution and accuracy. For calibration, commercially available TuneMix was used as well as the $^{DT}CCS_{N2}$ values published by Stow et al.[40] The source parameters were as follows: capillary voltage of 3.0 kV, a nebulizer pressure of 0.2 bar, dry gas temperature of 200 °C, and a dry gas flow of 3.5 L/min. Further details can be found in the Supporting Information.

Computational Details. *DFT Details.* The structure of the $Ag_{29}(BDT)_{12}(TPP)_4$ is known from X ray crystallography and was used as a starting point for our structure optimization after removal of the four TPP ligands.[10] Because these systems are quite large (173 atoms each), we used a small basis (Def2 SVP)[33] and functional (BP 86)[41] as implemented in the current version of Turbomole.[34] For the Cu exchange products, Ag atoms of the optimized Ag_{29} have been replaced with Cu atoms. Because the CCS in nitrogen is also

dependent on the charge distribution, an NPA[39] was performed on the optimized structures.

CCS Calculation Details. The CCS can be imagined as a rotationally averaged interaction area of the ion and the collision gas. This area depends on the ion and the collision gas and, among others, temperature and pressure. In our case, we used the trajectory method as implemented in IMoS 1.09,[36,37] which calculates the trajectory of the gas molecule. For our CCS calculations, we typically ran 4 500 000 trajectories. Further details are given in the Supporting Information.

.

AUTHOR INFORMATION

Corresponding Authors

Ananya Baksi − *Institute of Nanotechnology and Institute of Physical Chemistry, Karlsruhe Institute of Technology, 76344 Eggenstein Leopoldshafen, Germany;* orcid.org/0000 0003 3328 4399; Email: ananya.baksi@kit.edu

Manfred M. Kappes − *Institute of Nanotechnology and Institute of Physical Chemistry, Karlsruhe Institute of Technology, 76344 Eggenstein Leopoldshafen, Germany;* orcid.org/0000 0002 1199 1730; Email: manfred.kappes@kit.edu

Authors

Erik Karsten Schneider − *Institute of Physical Chemistry, Karlsruhe Institute of Technology, 76131 Karlsruhe, Germany*

Patrick Weis − *Institute of Physical Chemistry, Karlsruhe Institute of Technology, 76131 Karlsruhe, Germany;* orcid.org/0000 0001 7006 6759

Indranath Chakraborty − *Center for Hybrid Nanostructures (CHyN), University of Hamburg, 22761 Hamburg, Germany;* orcid.org/0000 0003 4195 9384

Olaf Fuhr − *Institute of Nanotechnology and Karlsruher Nano Micro Facility (KNMF), Karlsruhe Institute of Technology, 76344 Eggenstein Leopoldshafen, Germany*

Sergei Lebedkin − *Institute of Nanotechnology and Institute of Physical Chemistry, Karlsruhe Institute of Technology, 76344 Eggenstein Leopoldshafen, Germany*

Wolfgang J. Parak − *Center for Hybrid Nanostructures (CHyN), University of Hamburg, 22761 Hamburg, Germany;* orcid.org/0000 0003 1672 6650

Author Contributions

⊥A.B. and E.K.S. have contributed equally.

Author Contributions

A.B. and E.K.S. have jointly planned and performed the experiments and interpreted the results. P.W. helped in DFT calculation. O.F. has synthesized the $Cu_{12}S_6$ cluster and S.L. has characterized the cluster. The Ag_{29} cluster was synthesized in W.J.P. group under supervision of I.C. M.M.K. and A.B. wrote the manuscript with contribution from all authors. The whole project was supervised by M.M.K.

Notes

The authors declare no competing financial interest.

ACKNOWLEDGMENTS

M.M.K. and P.W. acknowledge support by the DFG funded Transregio collaborative research center "3MET" within project C6. M.M.K. is also grateful to KIT for funding of the tims TOFMS used in this study. The parts of this work from the group of W.J.P. were supported by the Cluster of Excellence "Advanced Imaging of Matter" of the Deutsche Forschungsgemeinschaft (DFG), EXC 2056, project ID 390715994. I.C. thanks Lizhen, Yuan, and Mustafa for help in Ag_{29} Synthesis.

REFERENCES

(1) Ferrando, R.; Jellinek, J.; Johnston, R. L. Nanoalloys: From Theory to Applications of Alloy Clusters and Nanoparticles. *Chem. Rev.* **2008**, *108*, 845−910.

(2) Gilroy, K. D.; Ruditskiy, A.; Peng, H. C.; Qin, D.; Xia, Y. Bimetallic Nanocrystals: Syntheses, Properties, and Applications. *Chem. Rev.* **2016**, *116*, 10414−10472.

(3) Jin, R.; Zeng, C.; Zhou, M.; Chen, Y. Atomically Precise Colloidal Metal Nanoclusters and Nanoparticles: Fundamentals and Opportunities. *Chem. Rev.* **2016**, *116*, 10346−10413.

(4) Chakraborty, I.; Pradeep, T. Atomically Precise Clusters of Noble Metals: Emerging Link between Atoms and Nanoparticles. *Chem. Rev.* **2017**, *117*, 8208−8271.

(5) Yan, N.; Liao, L.; Yuan, J.; Lin, Y. j.; Weng, L. h.; Yang, J.; Wu, Z. Bimetal Doping in Nanoclusters: Synergistic or Counteractive? *Chem. Mater.* **2016**, *28*, 8240−8247.

(6) Wang, S.; Li, Q.; Kang, X.; Zhu, M. Customizing the Structure, Composition, and Properties of Alloy Nanoclusters by Metal Exchange. *Acc. Chem. Res.* **2018**, *51*, 2784−2792.

(7) Ghosh, A.; Mohammed, O. F.; Bakr, O. M. Atomic Level Doping of Metal Clusters. *Acc. Chem. Res.* **2018**, *51*, 3094−3103.

(8) Hossain, S.; Niihori, Y.; Nair, L. V.; Kumar, B.; Kurashige, W.; Negishi, Y. Alloy Clusters: Precise Synthesis and Mixing Effects. *Acc. Chem. Res.* **2018**, *51*, 3114−3124.

(9) Joshi, C. P.; Bootharaju, M. S.; Alhilaly, M. J.; Bakr, O. M. $[Ag_{25}(SR)_{18}]^-$: The "Golden" Silver Nanoparticle. *J. Am. Chem. Soc.* **2015**, *137*, 11578−11581.

(10) AbdulHalim, L. G.; Bootharaju, M. S.; Tang, Q.; Del Gobbo, S.; AbdulHalim, R. G.; Eddaoudi, M.; Jiang, D. e.; Bakr, O. M. $Ag_{29}(BDT)_{12}(TPP)_4$: A Tetravalent Nanocluster. *J. Am. Chem. Soc.* **2015**, *137*, 11970−11975.

(11) Yang, H.; Wang, Y.; Huang, H.; Gell, L.; Lehtovaara, L.; Malola, S.; Hakkinen, H.; Zheng, N. All Thiol Stabilized Ag_{44} and $Au_{12}Ag_{32}$ Nanoparticles with Single Crystal Structures. *Nat. Commun.* **2013**, *4*, 2422.

(12) Desireddy, A.; Conn, B. E.; Guo, J.; Yoon, B.; Barnett, R. N.; Monahan, B. M.; Kirschbaum, K.; Griffith, W. P.; Whetten, R. L.; Landman, U.; Bigioni, T. P. Ultrastable Silver Nanoparticles. *Nature* **2013**, *501*, 399−402.

(13) Negishi, Y.; Munakata, K.; Ohgake, W.; Nobusada, K. Effect of Copper Doping on Electronic Structure, Geometric Structure, and Stability of Thiolate Protected Au_{25} Nanoclusters. *J. Phys. Chem. Lett.* **2012**, *3*, 2209−2214.

(14) Kang, X.; Wei, X.; Jin, S.; Yuan, Q.; Luan, X.; Pei, Y.; Wang, S.; Zhu, M.; Jin, R. Rational Construction of a Library of M_{29} Nanoclusters from Monometallic to Tetrametallic. *Proc. Natl. Acad. Sci. U. S. A.* **2019**, *116*, 18834−18840.

(15) Krishnadas, K. R.; Baksi, A.; Ghosh, A.; Natarajan, G.; Som, A.; Pradeep, T. Interparticle Reactions: An Emerging Direction in Nanomaterials Chemistry. *Acc. Chem. Res.* **2017**, *50*, 1988−1996.

(16) Krishnadas, K. R.; Natarajan, G.; Baksi, A.; Ghosh, A.; Khatun, E.; Pradeep, T. Metal Ligand Interface in the Chemical Reactions of Ligand Protected Noble Metal Clusters. *Langmuir* **2019**, *35*, 11243−11254.
(17) Khatun, E.; Chakraborty, P.; Jacob, B. R.; Paramasivam, G.; Bodiuzzaman, M.; Dar, W. A.; Pradeep, T. Intercluster Reactions Resulting in Silver Rich Trimetallic Nanoclusters. *Chem. Mater.* **2020**, *32*, 611−619.
(18) Krishnadas, K. R.; Baksi, A.; Ghosh, A.; Natarajan, G.; Pradeep, T. Manifestation of Geometric and Electronic Shell Structures of Metal Clusters in Intercluster Reactions. *ACS Nano* **2017**, *11*, 6015−6023.
(19) Bhat, S.; Baksi, A.; Mudedla, S. K.; Natarajan, G.; Subramanian, V.; Pradeep, T. $Au_{22}Ir_3(PET)_{18}$: An Unusual Alloy Cluster through Intercluster Reaction. *J. Phys. Chem. Lett.* **2017**, *8*, 2787−2793.
(20) Kazan, R.; Muller, U.; Burgi, T. Doping of Thiolate Protected Gold Clusters through Reaction with Metal Surfaces. *Nanoscale* **2019**, *11*, 2938−2945.
(21) Zhang, B.; Safonova, O. V.; Pollitt, S.; Salassa, G.; Sels, A.; Kazan, R.; Wang, Y.; Rupprechter, G.; Barrabes, N.; Burgi, T. On the Mechanism of Rapid Metal Exchange Between Thiolate Protected Gold and Gold/Silver Clusters: A Time Resolved *in Situ* XAFS Study. *Phys. Chem. Chem. Phys.* **2018**, *20*, 5312−5318.
(22) Baksi, A.; Chakraborty, P.; Bhat, S.; Natarajan, G.; Pradeep, T. $[Au_{25}(SR)_{18}]_2^{2-}$: A Noble Metal Cluster Dimer in the Gas Phase. *Chem. Commun.* **2016**, *52*, 8397−8400.
(23) Baksi, A.; Ghosh, A.; Mudedla, S. K.; Chakraborty, P.; Bhat, S.; Mondal, B.; Krishnadas, K. R.; Subramanian, V.; Pradeep, T. Isomerism in Monolayer Protected Silver Cluster Ions: An Ion Mobility Mass Spectrometry Approach. *J. Phys. Chem. C* **2017**, *121*, 13421−13427.
(24) Yang, X. X.; Issac, I.; Lebedkin, S.; Kuhn, M.; Weigend, F.; Fenske, D.; Fuhr, O.; Eichhofer, A. Red Luminescent Biphosphine Stabilized '$Cu_{12}S_6$' Cluster Molecules. *Chem. Commun.* **2014**, *50*, 11043−11045.
(25) Baksi, A.; Schneider, E. K.; Weis, P.; Krishnadas, K. R.; Ghosh, D.; Hahn, H.; Pradeep, T.; Kappes, M. M. Nanogymnastics: Visualization of Intercluster Reactions by High Resolution Trapped Ion Mobility Mass Spectrometry. *J. Phys. Chem. C* **2019**, *123*, 28477−28485.
(26) Hennrich, F.; Schneider, E.; Weis, P.; Kappes, M. M. Comparing Empty and Filled Fullerene Cages with High Resolution Trapped Ion Mobility Spectrometry. *J. Am. Soc. Mass Spectrom.* **2019**, *30*, 1973−1980.
(27) Weis, P.; Hennrich, F.; Fischer, R.; Schneider, E. K.; Neumaier, M.; Kappes, M. M. Probing the Structure of Giant Fullerenes by High Resolution Trapped Ion Mobility Spectrometry. *Phys. Chem. Chem. Phys.* **2019**, *21*, 18877−18892.
(28) Yan, J.; Su, H.; Yang, H.; Hu, C.; Malola, S.; Lin, S.; Teo, B. K.; Hakkinen, H.; Zheng, N. Asymmetric Synthesis of Chiral Bimetallic $[Ag_{28}Cu_{12}(SR)_{24}]^{4-}$ Nanoclusters *via* Ion Pairing. *J. Am. Chem. Soc.* **2016**, *138*, 12751−12754.
(29) Yang, H.; Wang, Y.; Yan, J.; Chen, X.; Zhang, X.; Hakkinen, H.; Zheng, N. Structural Evolution of Atomically Precise Thiolated Bimetallic $[Au_{12+n}Cu_{32}(SR)_{30+n}]^{4-}$ (n = 0, 2, 4, 6) Nanoclusters. *J. Am. Chem. Soc.* **2014**, *136*, 7197−7200.
(30) Song, Y.; Li, Y.; Li, H.; Ke, F.; Xiang, J.; Zhou, C.; Li, P.; Zhu, M.; Jin, R. Atomically Resolved $Au_{52}Cu_{72}(SR)_{55}$ Nanoalloy Reveals Marks Decahedron Truncation and Penrose Tiling Surface. *Nat. Commun.* **2020**, *11*, 478.
(31) Chakraborty, P.; Baksi, A.; Khatun, E.; Nag, A.; Ghosh, A.; Pradeep, T. Dissociation of Gas Phase Ions of Atomically Precise Silver Clusters Reflects Their Solution Phase Stability. *J. Phys. Chem. C* **2017**, *121*, 10971−10981.
(32) Perdew, J. P. Density Functional Approximation for the Correlation Energy of the Inhomogeneous Electron Gas. *Phys. Rev. B: Condens. Matter Mater. Phys.* **1986**, *33*, 8822.
(33) Weigend, F.; Ahlrichs, R. Balanced Basis Sets of Split Valence, Triple Zeta Valence and Quadruple Zeta Valence Quality for H to Rn: Design and Assessment of Accuracy. *Phys. Chem. Chem. Phys.* **2005**, *7*, 3297−3305.
(34) Furche, F.; Ahlrichs, R.; Hättig, C.; Klopper, W.; Sierka, M.; Weigend, F. Turbomole. *Wiley Interdiscip. Rev.: Comput. Mol. Sci.* **2014**, *4*, 91−100.
(35) Veenstra, A. P.; Monzel, L.; Baksi, A.; Czekner, J.; Lebedkin, S.; Schneider, E. K.; Pradeep, T.; Unterreiner, A. N.; Kappes, M. M. Ultrafast Intersystem Crossing in Isolated $Ag_{29}(BDT)_{12}^{3-}$ Probed by Time Resolved Pump Probe Photoelectron Spectroscopy. *J. Phys. Chem. Lett.* **2020**, *11*, 2675−2681.
(36) Larriba, C.; Hogan, C. J. Ion Mobilities in Diatomic Gases: Measurement *versus* Prediction with Non Specular Scattering Models. *J. Phys. Chem. A* **2013**, *117*, 3887−3901.
(37) Larriba, C.; Hogan, C. J. Free Molecular Collision Cross Section Calculation Methods for Nanoparticles and Complex Ions with Energy Accommodation. *J. Comput. Phys.* **2013**, *251*, 344−363.
(38) Warnke, S.; Seo, J.; Boschmans, J.; Sobott, F.; Scrivens, J. H.; Bleiholder, C.; Bowers, M. T.; Gewinner, S.; Schollkopf, W.; Pagel, K.; von Helden, G. Protomers of Benzocaine: Solvent and Permittivity Dependence. *J. Am. Chem. Soc.* **2015**, *137*, 4236−4242.
(39) Reed, A. E.; Weinstock, R. B.; Weinhold, F. Natural Population Analysis. *J. Chem. Phys.* **1985**, *83*, 735−46.
(40) Stow, S. M.; Causon, T. J.; Zheng, X.; Kurulugama, R. T.; Mairinger, T.; May, J. C.; Rennie, E. E.; Baker, E. S.; Smith, R. D.; McLean, J. A.; Hann, S.; Fjeldsted, J. C. An Interlaboratory Evaluation of Drift Tube Ion Mobility Mass Spectrometry Collision Cross Section Measurements. *Anal. Chem.* **2017**, *89*, 9048−9055.
(41) Perdew. Density Functional Approximation for the Correlation Energy of the Inhomogeneous Electron Gas. *Phys. Rev. B: Condens. Matter Mater. Phys.* **1986**, *33*, 8822−8824.